
Article:
John, E. orcid.org/0000-0002-8707-4197, Boxall, J. orcid.org/0000-0002-4681-6895, Collins, R. et al. (2 more authors) (2024) Fatigue failure analysis of grey cast iron water pipes accounting for fatigue strength variation. Engineering Failure Analysis, 165. 108762. ISSN 1350-6307

https://doi.org/10.1016/j.engfailanal.2024.108762

Engineering Failure Analysis 165 (2024) 108762

Contents lists available at ScienceDirect

Engineering Failure Analysis

journal homepage: www.elsevier.com/locate/engfailanal

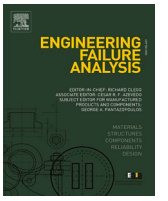

Fatigue failure analysis of grey cast iron water pipes accounting for fatigue strength variation

Edward John, Joby Boxall, Richard Collins, Elisabeth Bowman, Luca Susmel *

Department of Civil and Structural Engineering, The University of Sheffield, Sheffield, UK

ARTICLE INFO

Keywords:
Civil engineering
Water distribution pipe
Cast-iron
Casting
Mechanical testing
Fatigue
Maintenance error
Replacement

ABSTRACT

Fatigue cracking is thought to be a critical failure mode for Grey Cast Iron (GCI) water pipes; however, this failure mechanism is poorly understood. Using a novel approach to sourcing GCI pipe material for testing, the variation in fatigue strength between pipes from the same batch was experimentally quantified. These results were used to assess the impact of fatigue strength variation on a hypothetical but realistic GCI water pipe years-to-failure scenario. Full-pipe sections were used during fatigue testing and the observed failure mode gave physical meaning to the years-to-fatigue-failure predictions for the first time. The accumulation of fatigue damage was predicted to represent a terminal and very small part of a GCI pipe's life, so the loads applied to a GCI pipe early in its life are likely to have a limited impact on its remaining life and so do not need to be included in predictive modelling. For the scenario considered here, the predicted variation in lifetime was an 8.6-year range about an average of 59.4 years. GCI pipes in the UK are all > 50 years old, so this is a significant variation for asset and investment planners to account for as these pipes approach the end of their lives.

1. Introduction

Failure of water distribution pipes is a major cause of water loss, leading to leakage rates of around 20 % in the UK [1] and between 10 % and 20 % in many US states [2]. Reducing leakage rates is essential so that the resilience of water supplies can be improved in the face of increasing populations and less-predictable rainfall [3]. Pipes made of Grey Cast Iron (GCI) are common in many UK and North American networks and are often identified as having high failure rates [2,4,5]. Despite all GCI pipes in the UK being at least 53 years old [6], low pipe replacement rates in the UK (0.1 % per year) and US (average 0.8 % per year) mean it is unlikely that GCI water pipes will be entirely removed from service in the foreseeable future [2,7]. As a result, it is essential to understand how these pipes fail and develop techniques to predict their remaining life so that the greatest reduction in leakage can be achieved with present pipe replacement rates.

A defining feature of GCI is the graphite flake inclusions contained within its microstructure. As well as giving GCI its grey colour the graphite flakes act as internal defects, giving GCI highly brittle tensile behaviour, and enable graphitic corrosion [8–10]. Graphitic corrosion is thought to spread from graphite flakes and replaces the surrounding iron matrix with a much weaker corrosion product and can take the form of deep pits or wide patches [9–12]. The significantly lower strength of the corrosion product means that the pipe's wall thickness is effectively reduced in regions subject to corrosion, resulting in higher pipe wall stresses occurring for a given

* Corresponding author.
E-mail addresses: edajohn1@sheffield.ac.uk (E. John), j.b.boxall@sheffield.ac.uk (J. Boxall), p.collins@sheffield.ac.uk (R. Collins), bowman@sheffield.ac.uk (E. Bowman), l.susmel@sheffield.ac.uk (L. Susmel).

https://doi.org/10.1016/j.engfailanal.2024.108762
Received 28 May 2024; Received in revised form 5 August 2024; Accepted 10 August 2024
Available online 11 August 2024

Nomenclature

a	Corrosion model constant (year^{-1})
a_{cr}	Critical crack half-length (m)
c	Corrosion model constant (year^{-1})
D_i	Fatigue damage caused during the i-th time increment
d_P	Corrosion depth (mm)
f	Loading frequency (year^{-1})
K	Material fatigue curve negative inverse slope
K_{IC}	Material fracture toughness (Pa•m$^{1/2}$)
k	Corrosion model constant (mm)
N_A	High-cycle reference stress cycles to failure
N_f	Stress cycles to failure
P_i	Internal water pressure (Pa)
P_{max}	Maximum pressure (Pa)
P_{min}	Minimum pressure (Pa)
P_S	Probability of survival
p_i	Cumulative probability
q	S-N curve probability of survival factor
r_i	Pipe initial inside radius (mm)
r_o	Pipe initial outside radius (mm)
$\widehat{s}$	Estimated standard deviation
$T\sigma$	Stress amplitude scatter
t	Time (years)
t_i	Studentised residual
Δt	Time increment (years)
ε	Strain (mm/mm)
σ_A	Material high-cycle reference stress amplitude determined at N_A (Pa)
$\sigma_{A,P_s=P\%}$	σ_A for a P% probability of survival (Pa)
σ_a	Applied stress amplitude (Pa)
$\sigma_{a,R=-1}$	Equivalent fully-reversed uniaxial stress amplitude (Pa)
σ_{max}	Maximum applied stress (Pa)
σ_n	Global stress applied normal to a crack (Pa)
σ_θ	Hoop stress (Pa)

load [13–15]. Therefore, provided the loads experienced by a pipe are of a sufficient magnitude, the formation of a crack at the base of a corrosion pit can be the primary failure mechanism for GCI water pipes [16].

Several previous studies have proposed deterministic approaches to predict years-to-failure caused by cracking for GCI pipes subject to static loading [13,15] and fatigue loading [17,18]. Brevis *et al.* [17] and Jiang *et al.* [18] both found that in certain circumstances fatigue cracking may be the critical failure mode of GCI water pipes, however, this failure mode is poorly understood. The fatigue cracking years-to-failure models require the material's fatigue curve as an input, however, significant variations in material properties are often observed between coupons taken from the same pipe [18–22] which adds uncertainty to these model's predictions. The pipe failure mode predicted by previous years-to-fatigue-failure models is unclear because the fatigue curves were derived from reference values or dog-bone tests [17,18].

It is not currently known whether the variation in fatigue strength between pipes from the same batch (nominally identical pipes cast by the same foundry and installed at the same time) introduces significant uncertainty to the predicted the years-to-failure. Therefore, this study aimed to experimentally quantify the variation of fatigue strength observed within a batch of GCI pipes and assess the impact of this variation on a years-to-failure scenario.

To achieve the above aim fatigue tests of material from GCI pipes produced by the same manufacturer were required. Sourcing exhumed pipes meeting this requirement was not possible as continuous lengths of pipeline are not usually removed at once and the provenance of exhumed pipes is rarely known. A potential alternative to exhumed GCI water pipes for destructive testing was off-the-shelf soil pipes made in accordance with BS 416–2 [23], which were easy to obtain, manufactured from GCI, and were available with nominal diameters from 50 mm to 150 mm. The graphite microstructure and tensile stress–strain behaviour of GCI can be used to distinguish different types of GCI and have links to the material's fatigue behaviour [8,20,24] so these properties of the new BS 416–2 pipes were characterised to investigate whether BS 416–2 soil pipes can be used to represent GCI water pipes in small-scale destructive experiments.

2. GCI water pipe material properties from literature

To facilitate comparison of the new BS 416–2 pipes with in-service GCI water pipes this section reviews the graphite microstructure and tensile stress–strain literature data for exhumed GCI water pipes. The size and distribution of graphite flakes is known to strongly affect the material's mechanical properties, with larger flakes generally resulting in a lower bulk tensile strength [20]. The size and distribution of graphite flakes is determined by the chemical composition of the GCI and the rate at which the iron cooled, with slower cooling generally allowing larger flakes to form [8]. The cooling rate can be influenced by the pipe's wall thickness, the ambient temperature, and the manufacturing process used.

GCI pipes broadly fall into two categories which are determined by the manufacturing technique used. In the UK, pit-cast iron pipes were manufactured from the mid-1800 s until the 1920 s using vertical sand moulds, which generally resulted in slow cooling times and larger graphite flakes. Spun-cast pipes were manufactured from the 1920 s to 1960 s and were cast in horizontal, spinning, water-cooled metal moulds, resulting in fast cooling times and smaller graphite flakes [5,6,25,26]. UK water utilities frequently report that their distribution networks contain more spun-cast grey iron pipes than pit-cast grey iron pipes, and water utility data sets shown to the author support this. Spun-cast grey iron pipes are likely more prevalent due to their more recent installation period.

Most previous works report the graphite flake morphology and sizes of the GCI pipes examined according to ASTM A247-19 [27] or a preceding version of the standard. A247-19 describes the graphite microstructure according to its size, form, and distribution.

Literature data for pit-cast iron pipes give flake sizes of between Class 5 and Class 1, or 40 μm to $\geq$ 640 μm, with the large flakes tending to occur in the central region of the pipe wall [8,20,28]. Similar data for spun-cast pipes gives sizes between Class 8 and Class 4, or $<$ 10 μm to 160 μm, with the larger flakes often occurring towards the inside wall of the pipe [8,20,28]. These size ranges therefore broadly match the theory that pit-cast pipes should have larger flakes than spun-cast pipes. The trends across the pipe walls also suggest that the centre of the wall cools most slowly in pit-cast pipes, whereas the inside wall cools most slowly in spun-cast pipes.

Literature reports of stress–strain tests using exhumed GCI pipes come mainly from North America and Australia and are predominantly for spun-cast pipes [8,9,18,20,29]. Boxplots of the available tensile stress–strain parameters for GCI pipes are provided in Fig. 1. The spread of Ultimate Tensile Strengths (UTSs) observed for spun-cast pipes is significant with a range of 130 to 305 MPa. As expected from the microstructural differences, the UTSs reported for pit-cast pipes are generally lower than for spun-cast pipes, falling within the range 68 to 188 MPa.

Failure strains are less frequently reported by literature sources, however Makar and McDonald [20] concluded from their tests that spun-cast pipes generally have higher failure strains than pit-cast pipes. The same study also found that the stress–strain response of spun-cast GCI often features a "knee", indicating a degree of plastic yielding, whereas pit-cast material does not. As a result, the 0.2 % offset yield strength can be calculated for some spun-cast pipes, as shown in Fig. 1. Regarding the elastic stress–strain response, spun-cast pipes generally seem to have higher initial elastic moduli than pit-cast pipes, although there is very little data for pit-cast pipes [20,29].

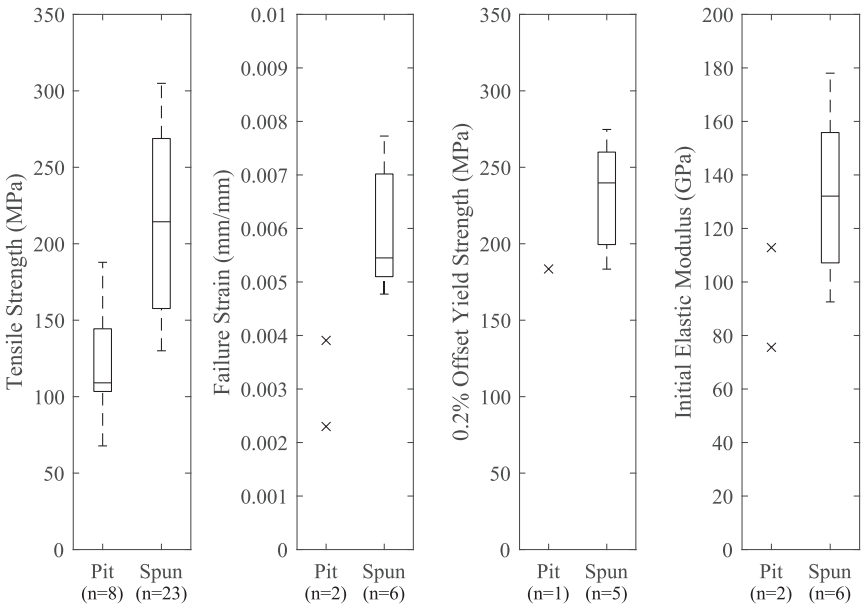

Fig. 1. Box plots of the GCI water pipe tensile stress–strain data available from the literature grouped by casting technique [8,9,18,20]. Crosses mark individual data points where the data set is small.

3. Materials and methods

3.1. Material characterisation

BS 416–2 DN50 soil pipes (product code MS2001 [30]) manufactured by Hargreaves Foundry (Halifax, UK) were obtained so that the properties of the pipe could be characterised and compared with the literature data for exhumed GCI water pipes. These pipes were supplied with a thin coat of yellow paint on their internal surfaces which was not removed for testing because of the negligible strength of the paint. Characterisation of the fatigue properties of the material is reported by John *et al.* [31]. DN50 was selected because these pipes were intended for use in scaled-down tests where a small diameter is beneficial. The manufacturer confirmed that the pipe supplied was manufactured using a centrifugal casting process (spin-casting) in a water-cooled metal mould.

3.1.1. Microscopy

The microscope inspection aimed to characterise the graphite microstructure of the material across the full thickness of the pipe wall. Three small material samples were cut from the pipes and polished. ASTM standard A247-19 [27] was adhered to for evaluation of the graphite microstructure. To capture the expected variation in flake size across the pipe wall a series of images were taken in a straight line spanning from the outside wall to the inside wall. This was repeated for the three material samples, with a total image count of 21 for the first sample and 33 each for the second two samples. The intervals between the images for a given specimen were approximately equal.

Each image was processed using the MatLab Image Processing Toolkit [32] to determine the length and area of the graphite present. A247-19 [27] does not specify the process for measuring flake length, so the largest straight-line distance between any pair of points around the flake edge was used. Objects smaller than 1 μm were excluded as it was not possible to confirm whether these were graphite or other features due the resolution of the images. The results from the three samples were combined to provide a more representative view of the pipe's graphite microstructure.

3.1.2. Tensile testing

To ensure that the UTS measured reflected the fatigue specimens tested by John *et al.* [31], the same specimen geometry (Fig. 2) and testing arrangement were used. Three randomly selected specimens were tested. To determine the applied strains, a 25 mm gauge length extensometer was attached to the specimens during these tensile tests. Due to the highly brittle nature of the material, a low displacement rate of 0.09 mm/minute was used to conduct the tensile tests to ensure that the stress–strain curve was captured with a sufficient resolution of data points. The brittle failure mode of the material meant no noticeable necking of the tensile specimens occurred, so post-test fracture surface calliper measurements, excluding the paint thickness, were used to determine the cross-sectional area of each specimen. The area of each specimen was assumed to remain constant throughout the test and was used to calculate the applied stress.

3.2. Fatigue testing

Years-to-failure modelling based on fatigue cracking requires the material's uniaxial fatigue curve [17,18]. This may be determined by fitting a curve to data generated by testing specimens to failure at a range of cyclic stress amplitudes [33,34]. The variance of the material's fatigue behaviour can be estimated from the difference between the observations and predictions of the fitted curve [35]. To enable the variance of fatigue strength within a pipe cohort to be estimated, the fatigue data used to determine the uniaxial fatigue curve was generated using specimens drawn from across several pipes, rather than from a single pipe.

63 fatigue specimens (Fig. 2) were produced from 7 new BS416-2 soil pipes sourced from the same foundry. Tubular specimens were used so that the fatigue cracking behaviour would be more representative of a water pipe. 18 randomly selected tubular fatigue specimens were tested under uniaxial fully reversed loading with the remaining specimens tested under other load conditions not reported here, as described by John et al. [31]. The fracture surface of each specimen was visually inspected post-test for features of

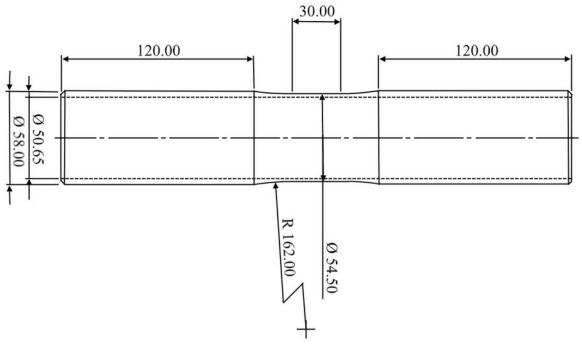

Fig. 2. Fatigue specimen geometry from John et al. [31].

interest

The 50 % probability of survival (P_s) S-N curve was determined using the least-squares method, in accordance with ASTM E739-10 [34]. The $P_s = 10$ % and $P_s = 90$ % curves were calculated from the $P_s = 50$ % curve according to the following relation, given by ASTM STP-91 [35]:

$$\sigma_{A,P_s=P\%} = \sigma_{A,P_s=50\%}\left\{\frac{N_A}{10^{\left[log_{10}(N_A)+q\hat{s}\right]}}\right\}^{1/K} \tag{1}$$

To calculate $\sigma_{A,P_s=P\%}$ using Eq. (1), for a particular probability of survival, the appropriate value of the factor q must be selected from table 33 of reference [35]. To test the fatigue data for a normal distribution a normal probability plot of the Studentised residuals vs the cumulative probability was used according to Montgomery *et al.* [36].

3.3. Years-to-failure predictions

For the years-to-failure modelling a 6″ Class D spun cast BS1211:1958 [26] pipe ($r_o = 88.5mm$, $r_i = 77.6mm$) was assumed to suffer uniform external wall loss corrosion, as illustrated by Fig. 3. The assumption that corrosion of GCI pipes can be equated to uniform wall loss is often used [13–15] and can be justified for the present application by the very low fatigue notch sensitivity of GCI [37–39].

The exponential corrosion model proposed by Rajani *et al.* [40] was used to estimate the corrosion depth at any given time:

$$d_P(t) = at + k(1 - e^{-ct}) \tag{2}$$

Brevis *et al.* [17] and Jiang *et al.* [18] both found that the life reduction caused by fatigue damage was more significant in low-corrosion scenarios, so the corrosion constants were assumed to take the values recommended by Rajani et al. [40] for low corrosion rates ($a = 0.021$, $k = 9.75$, and $c = 0.058$).

The assumed loading was constant amplitude pressure variations with $P_{max} = 441$ kPa, $P_{min} = 98$ kPa, and $f = 1.14\text{x}10^5$/year, similar to those reported by Rezaei et al. [41]. The hoop stress experienced by the pipe for any given corrosion depth was calculated using the thick-walled pressure vessel relations for an open-ended pressure vessel, but modified to account for wall the thickness reduction due to corrosion:

$$\sigma_\theta(t) = \frac{2r_i^2 P_i}{\left[r_o - d_p(t)\right]^2 - r_i^2} \tag{3}$$

The assumed loading had a non-zero mean stress, whereas the experimental data was generated under fully reversed loading. GCI is sensitive to the presence of mean stresses during fatigue loading; however, the Smith-Watson-Topper (SWT) criterion has previously been found effective at predicting the mean stress effect in GCI [31,42]. Therefore, the mean stress was accounted for using the stress-based variant of the SWT criterion [43], given by:

$$\sigma_{a,R=-1}(t) = \sqrt{\sigma_{max}(t)\sigma_a(t)} \tag{4}$$

The equivalent fully reversed uniaxial stress amplitude returned by the SWT criterion was then used to calculate the number of load cycles that would be required to cause fatigue failure using Eq. (5) [44]. Corrosion pit depth was calculated in 0.1-year time steps and the fatigue damage associated with each 0.1-year time step was calculated using Miner's rule (Eq. (6) [44]. Fatigue failure was assumed to occur in the first time increment where the sum of fatigue damage from that time increment and all previous time increments exceeded 1.

$$N_f(t) = N_A\left(\frac{\sigma_A}{\sigma_{a,R=-1}(t)}\right)^K \tag{5}$$

$$D_i = \frac{f\Delta t}{N_f(t)} \tag{6}$$

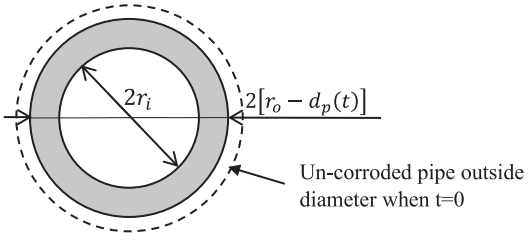

Fig. 3. Assumed pipe cross-section geometry for uniform external corrosion. The outside radius is taken to reduce with time due to corrosion whereas the internal radius is constant.

To investigate the variation of fatigue strength on predicted years-to-failure, randomised values of the material high-cycle reference stress amplitude, σ_A, were generated and the predicted years-to-failure was calculated for each value. Specifically, 10^4 values of σ_A were drawn from the random normal distribution having the same mean and variance as the BS416-2 pipe fatigue data set generated for this work. This ensured that the distribution of σ_A values used represented the observed variation within a batch of pipes. The negative inverse slope, K, of the fatigue curves were assumed to be constant and always equal to the average value of the experimental data.

4. Results

4.1. Graphite microstructure

The majority of graphite observed in the BS416-2 pipe fell into ASTM A247-19 [27] size Class 8 (<10 μm), with some larger Class 7, 6, and 5 flakes also present. As shown by Fig. 4, the breakdown of graphite size was found to be very similar for the two quarters of the wall closest to the outside surface, with Class 8 graphite making up around 85 % of the total graphite area, and slightly more than 1 % of the area being Class 6. The largest graphite was found to occur closer to the inside wall, with about 3.5 % of the graphite area in the wall quarter closest to the inside edge being Class 5. The largest individual piece of graphite observed in this region was 76.6 μm long.

The graphite observed in the BS416-2 pipe was mainly Type VII flake graphite (see Fig. 5), with a small amount of Type III compacted graphite present near the inside wall of the pipe. Where Type III graphite occurred it was mainly found near regions of iron devoid of graphite, such as the example shown in Fig. 5d. Note that in the top region of Fig. 5d the faint white lines may indicate the presence of pearlite.

Nearly all observations made in the mid-region of the pipe wall showed Distribution D graphite (very fine flakes surrounded by areas without graphite, see Fig. 5b). Around 10 % of observations near the outside wall and more than 60 % of the observations near the inside wall were Distribution A or C (uniformly distributed randomly oriented flakes or randomly oriented flakes of widely varying sizes, see Fig. 5a and 5c).

4.2. Tensile stress–strain tests

An example of a failed tensile test specimen is shown by Fig. 6 and the stress–strain curves calculated for the three tensile tests are shown by Fig. 7. The stress–strain curves show very brittle behaviour with no discernible yielding. For each specimen failure was total and sudden with no measurable elongation after the UTS was achieved.

The values of elastic modulus and stress and strain at the 0.2 % yield point and UTS point are given in Table 1.. The 0.2 % offset yield point could only be determined for test 2 as the other tests failed at very low strains meaning that the stress–strain curve did not intercept the 0.2 % offset line. All three tests gave similar elastic moduli and UTS values. The average values of elastic modulus and UTS were 82.11 GPa and 229.0 MPa, respectively. The failure strain varied substantially and the lowest failure strain was nearly half the largest failure strain.

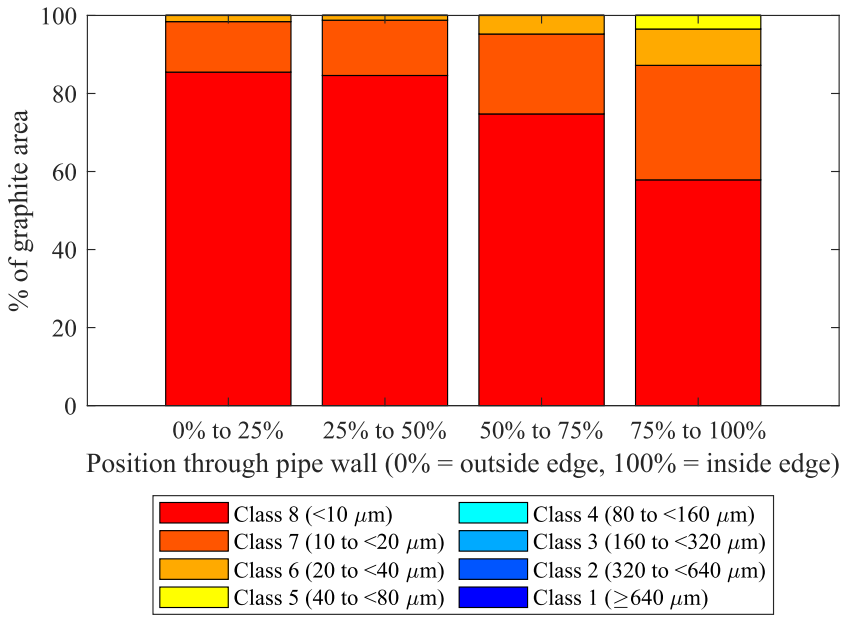

Fig. 4. Proportion of graphite, by area, in each ASTM A247-19 [27] size class across the wall of the BS 416–2 pipe.

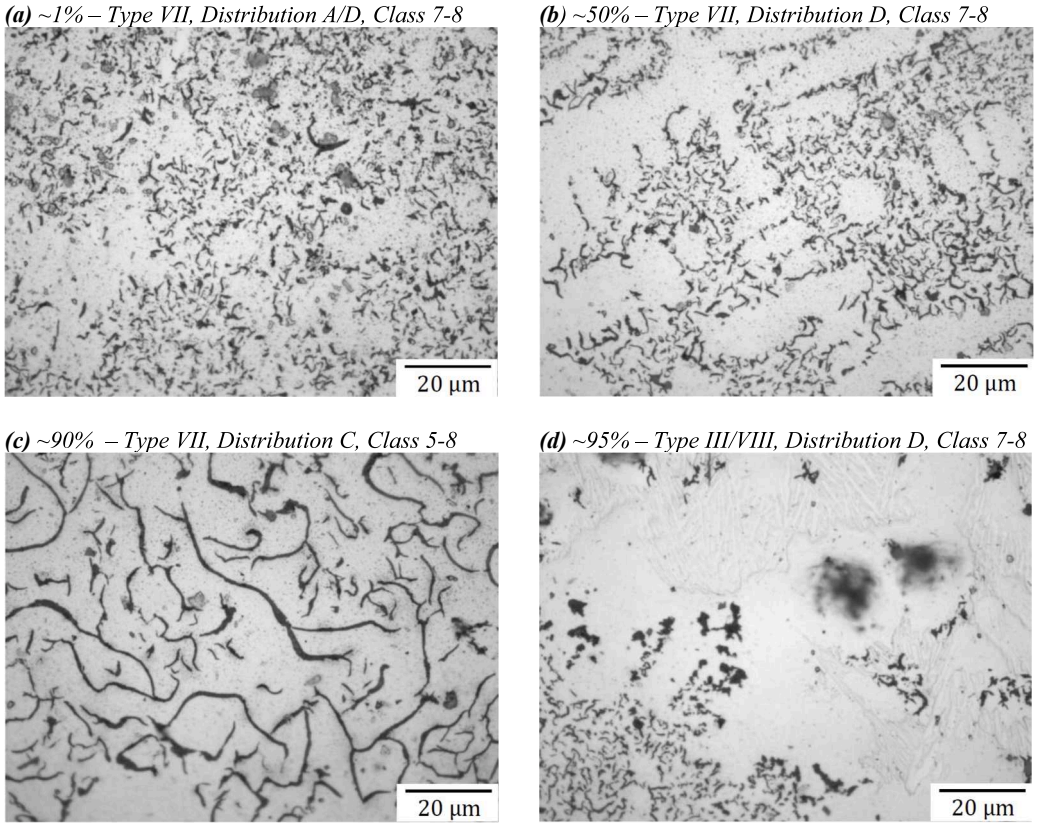

Fig. 5. Selection of optical microscope images showing the graphite microstructure of the BS416-2 pipe. ~ X% refers to the approximate position of the image, where ~ 0 % would be the outside wall and ~ 100 % would be the inside wall.

4.3. Fatigue tests

The fatigue data reported in Fig. 8 were originally reported by John et al. [31], however, for this analysis the 4 specimens which featured visible casting defects on the fracture surface were included in the statistical analysis as in-service water pipes also contain casting defects [5]. 2 specimens survived 2x10^6 cycles and were classed as runouts, and so were excluded from the statistical analysis. $\sigma_{A,P_s=90\%}$ was calculated to be 52.2 MPa, for $N_A = 10^6$ and a confidence factor of 0.95.

The calculated $P_s = 50$ % fatigue curves, normalised by UTS, for these data and the GCI water pipe tested by Kommers [19] were similar. The $T\sigma$ value ($P_s = 10$ % stress amplitude / $P_s = 90$ % stress amplitude, both at 10^6 cycles), which provides a measure of scatter [45], for the new data was 2.14, compared to 1.25–1.42 for fatigue data obtained from a single pipe [18,19]. This higher Tσ is likely accounted for by the fact that specimens containing defects were included in the data set and that fatigue specimens were drawn from a batch of pipes, rather than a single pipe as was the case for Jiang *et al.* [18] and Kommers [19].

4.4. Fatigue specimen fracture surface analysis

Fig. 9 shows a representative selection of failed uniaxial fatigue specimens and Fig. 10 shows detailed views of two typical fracture surfaces. In all cases the fracture direction was circumferential, meaning the crack grew on the plane of maximum normal stress amplitude.

A common feature, present on many uniaxial fatigue fracture surfaces, was a section with lower roughness than most of the fracture surface which appeared a lighter shade of grey. Where present, these light grey regions spanned the full wall thickness of the specimens. It was hypothesised that, due to their lower surface roughness, these regions indicated the location of crack initiation and stable crack growth before the crack grew to such a size that unstable crack growth caused specimen failure, as illustrated by Fig. 10. Fig. 11 shows optical microscope images from two specimens that further illustrate the lower roughness of the hypothesised stable crack growth regions, relative to the rest of the fracture surface. Another common fracture surface feature was a crack penetrating at a shallow angle below the fracture surface. This crack was typically about 180° from the likely stable crack growth region, so it was interpreted as the point that the two crack tips met, with some misalignment, having propagated around the specimen. This is also illustrated by Fig. 10.

To test the idea that the observed light grey fracture surface regions were regions of stable crack growth the length of each light grey

Fig. 6. Image showing a failed tensile test specimen. Note that the extensometer was repositioned for the photograph.

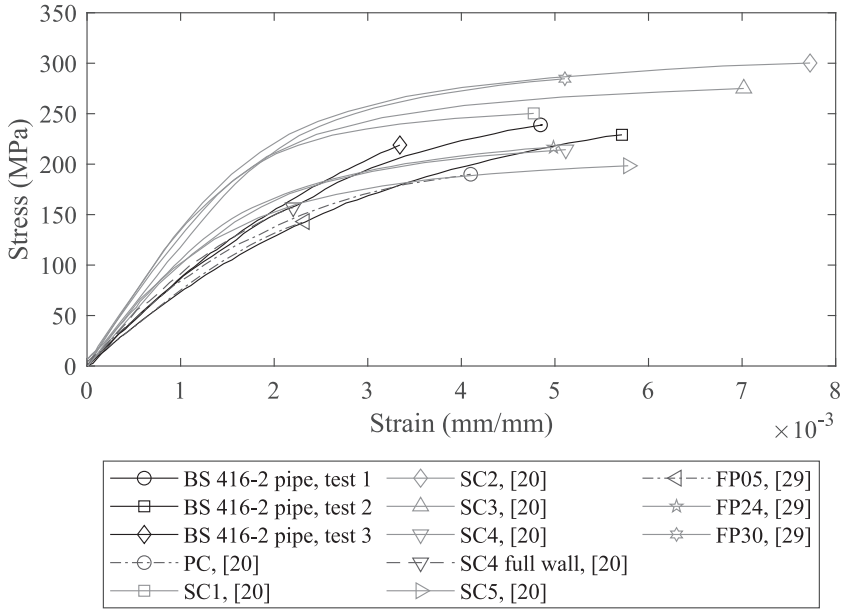

Fig. 7. Tensile stress–strain curves for the three BS416-2 pipe tensile specimens tested and available literature exhumed GCI water pipe stress–strain curves for comparison. The marker on each curve indicates the point that failure occurred.

Table 1
Tensile stress–strain test parameters for the three BS 416–2 pipe tensile specimens tested.

Test	Area (mm^2)	Elastic modulus (GPa)	0.2 % yield point		Failure	
			Stress (MPa)	Strain (με)	Stress (MPa)	Strain (με)
1	297.7	85.60	–	–	238.9	4.846
2	310.3	75.60	215.2	4.847	229.1	5.716
3	245.6	85.14	–	–	218.9	3.343
Mean		82.11			229.0	4.635

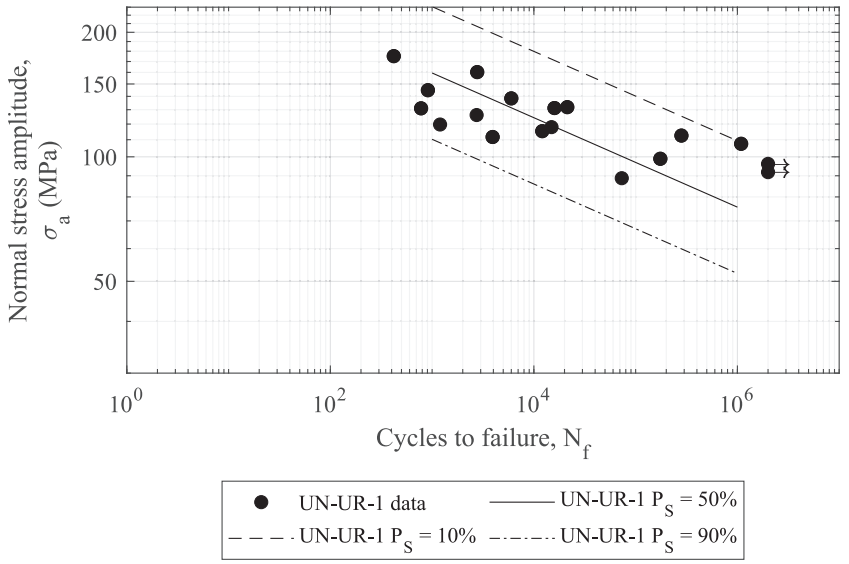

Fig. 8. Fully reversed uniaxial fatigue data (UN-UR-1) from John et al. [31] generated by testing specimens produced from a batch of GCI pipes. 10%, 50%, and 90% P_S lines are shown.

region was measured and compared with the critical crack length for fast fracture predicted by the Linear Elastic Fracture Mechanics equation for the critical crack length of a through-thickness crack in an infinite plate [46]:

$$a_{cr} = \frac{1}{\pi}\left(\frac{K_{IC}}{\sigma_n}\right)^2 \tag{7}$$

As the fracture toughness of the specimens was not known the average fracture toughness reported by Makar and Rajani [8] for exhumed spun cast grey iron pipes (13.8 MPa•$m^{1/2}$) was used. The predicted crack length for fracture ($2a_{cr}$) is plotted against the measured stable crack growth region for each uniaxial fatigue specimen on Fig. 12. The measured stable crack growth region is also plotted against cycles to failure in Fig. 13. Measured stable crack growth region length is reported as zero where no light grey region was discernible.

4.5. Years-to-failure predictions

Fig. 14 shows the normal probability plot of the fatigue data from Fig. 8. The Studentised residuals and cumulative probabilities plotted in Fig. 14 were calculated from $\log N_f$ and $\log\sigma_A$. The data points in Fig. 14 follow the linear regression fit closely without a definite skew at either end of the distribution, indicating that the fatigue data shown in Fig. 8 has a normal distribution within log–log space [36]. Therefore, values of $\log\sigma_A$ were drawn from the random normal distribution with same mean and variance as the fatigue data in log–log space, for $N_A = 10^6$. Fig. 15 shows the distribution of the σ_A values used in the years-to-failure calculations. Note that the skewed distribution of σ_A values resulted from converting the values of $\log\sigma_A$ to σ_A. The negative inverse slope of the experimental data, used in Eq. (5) to make fatigue life predictions, was 9.05.

Fig. 16 illustrates the distribution of predicted years-to-failure. 90 % of failures were predicted to occur within a range of 3.4 years and 100 % of failures were predicted to occur within a range of 8.6 years, which is a small variation relative to the average 59.4 years-to-failure prediction.

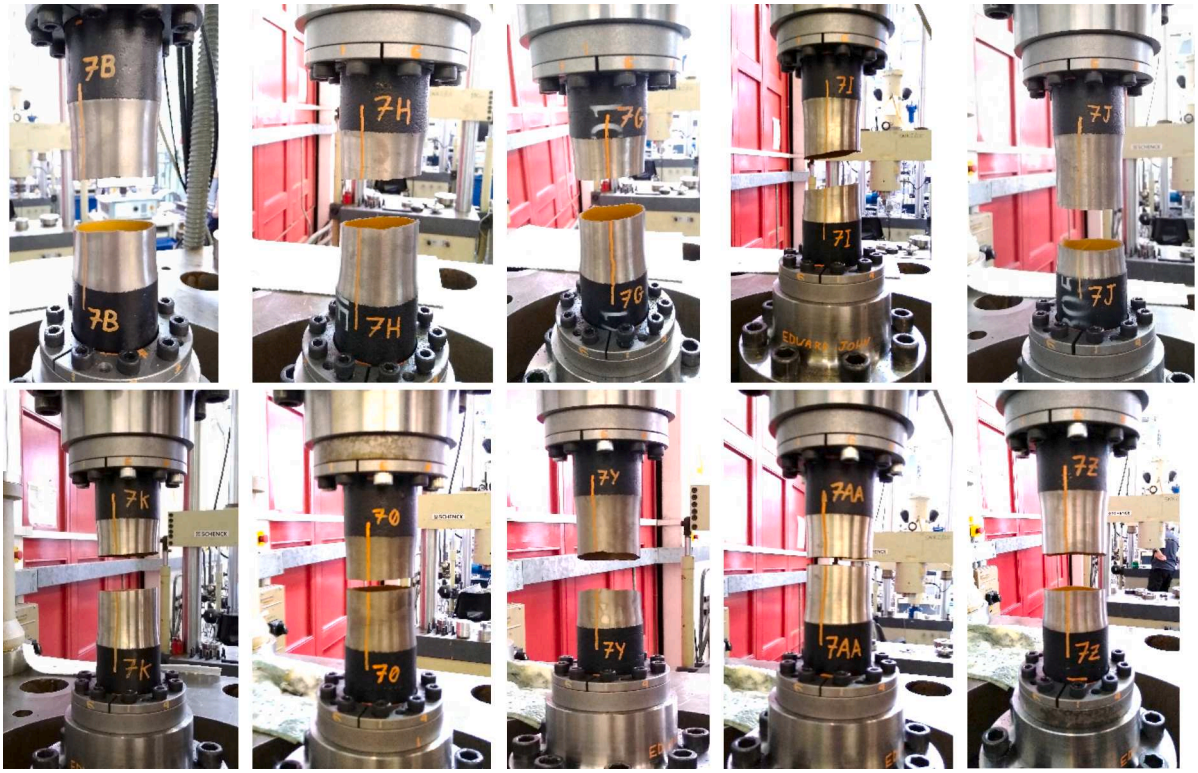

Fig. 9. Images showing a representative selection of failed uniaxial fatigue specimens for which the fatigue data is shown by Fig. 8.

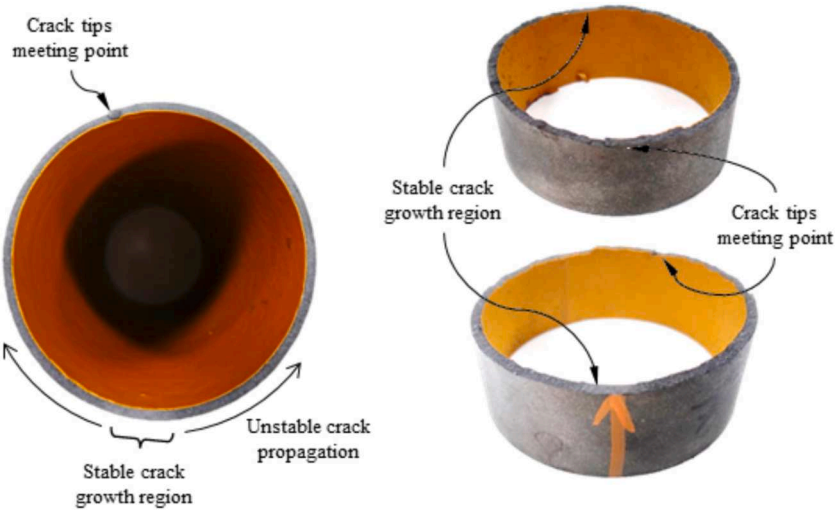

Fig. 10. Labelled photographs showing the fracture surfaces of two specimens tested under uniaxial fatigue. The two right-hand images show the same specimen rotated through 180°.

5. Discussion

5.1. Comparison of new pipe properties with exhumed pipes

The graphite sizes, types, and distributions observed in the BS416-2 pipe matched the literature data for spun-cast water pipes well. The outer and middle regions of the pipe wall were dominated by fine (Class 8 and Class 7), Distribution D, Type VII graphite flakes (Fig. 5b) which are typical of spun-cast pipes examined by previous authors [8,9]. The region of cast iron closest to the inside wall of

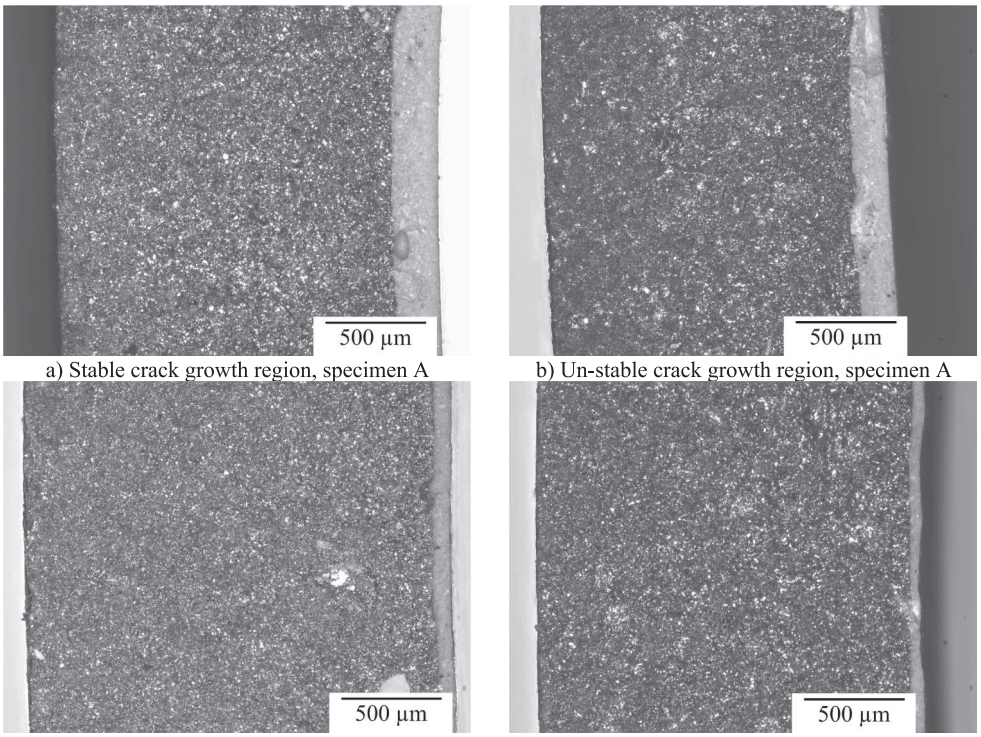

a) Stable crack growth region, specimen A
b) Un-stable crack growth region, specimen A
c) Stable crack growth region, specimen B
d) Un-stable crack growth region, specimen B

Fig. 11. Optical microscope fracture surface images at × 5 magnification. Note that the strip on the right of each image is a layer of paint.

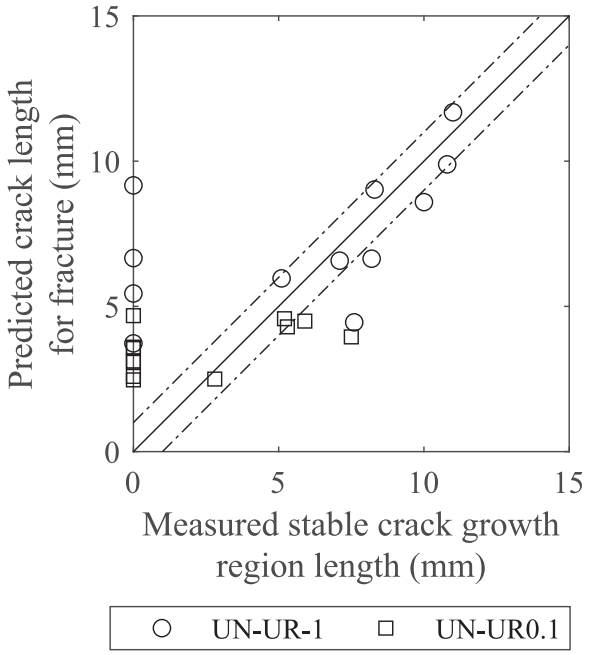

Fig. 12. Crack length for unstable fracture ($2a_{cr}$) plotted against the measured stable crack growth region for un-notched uniaxial tests. "UN-UR-1" are un-notched uniaxial R=-1 fatigue data and "UN-UR0.1" are un-notched uniaxial R=0.1 fatigue data from John et al. [31]. The solid line indicates perfect prediction while the dash-dot lines indicate a range of ± 1 mm from perfect prediction.

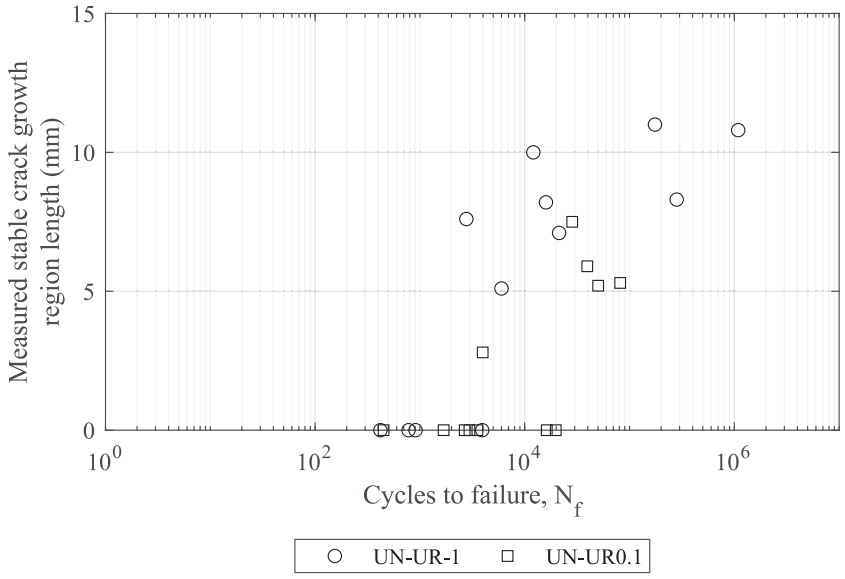

Fig. 13. Measured stable crack growth region plotted against cycles to failure for un-notched uniaxial tests. "UN-UR-1" are un-notched uniaxial R=-1 fatigue data and "UN-UR0.1" are un-notched uniaxial R=0.1 fatigue data from John et al. [31].

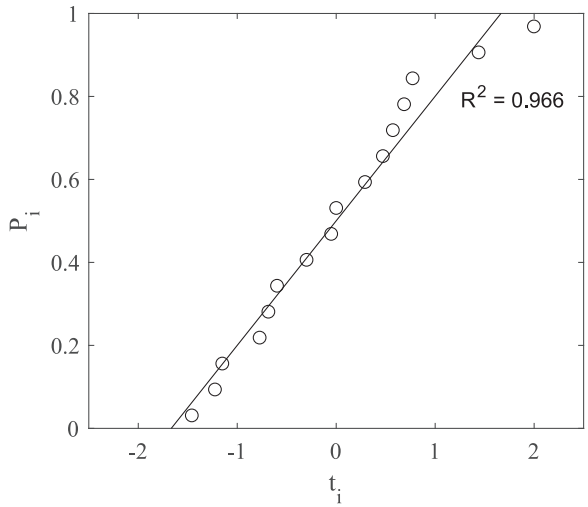

Fig. 14. Normal probability plot of the data from Fig. 7 and the least squares linear regression fit, where t_i is the Studentised residual and p_i is the cumulative probability.

the pipe varied from this norm, with ~ 500 μm diameter patches of Distribution A or C, Type VII flakes with sizes up to Class 5 (Fig. 5c). These areas with large flake sizes were likely due to the longer cooling time experienced by the iron closest to the inside wall, giving more time for larger flakes to form, and are consistent with observations in the literature [8,9]. Also found close to the inside wall were possible areas of pearlite, surrounded by Type III compacted graphite (Fig. 5d). Pearlite grains are associated with cast iron that has cooled more slowly [8] and Type III graphite is reportedly common in annealed malleable iron castings [27]. Therefore, the occurrence of the regions containing pearlite and Type III graphite was also probably associated with the slower cooling rate of the pipe inside wall.

The measured UTS of the BS 416–2 pipe tensile specimens fell centrally within the 130 to 305 MPa range reported for spun cast pipes in the literature. The failure strains of tests 1 and 2 were at the lower end of the expected range for spun cast pipes and the failure strain of test 3 was lower than the expected range. The initial elastic moduli of all three BS 416–2 tensile tests were lower than those reported for exhumed spun cast pipes and were more typical of the values associated with pit cast pipes.

These literature tensile stress–strain properties reported are usually from the strongest specimens tested from each pipe which the references highlight as representative [20,29]. Fortunately, Makar and McDonald [20] provide the data from repeat tests for two of the spun-cast pipes they investigated ("SC2" and "SC4"). Makar and McDonald [20] observed that some specimens which sampled the full

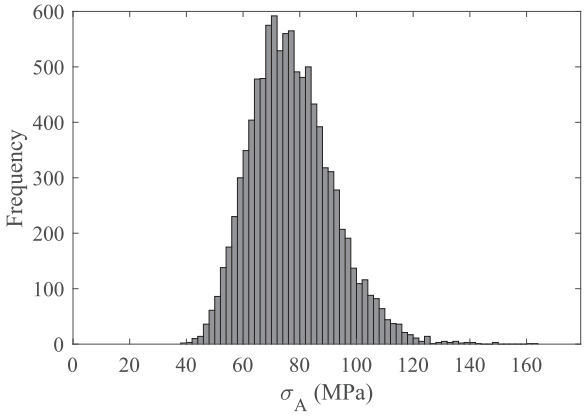

Fig. 15. Histogram showing the distribution of the 10^4 values of material high-cycle reference stress amplitude, σ_A, used to make years-to-failure predictions.

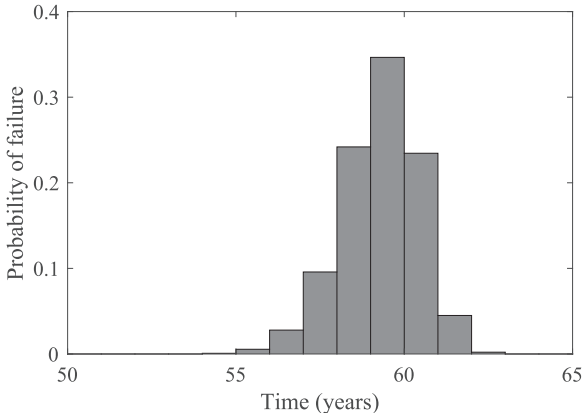

Fig. 16. Histogram showing the distribution of predicted years-to-failure corresponding to the 10^4 randomly generated values of fatigue strength.

wall thickness of their spun-cast pipes failed at strains around 0.002 mm/mm (an example of which is plotted in Fig. 7 as "SC4 full wall") while specimens from the same pipe which only sampled the outside 50 % of the pipe wall failed at strains between around 0.004 and 0.008 mm/mm. Additionally, some full wall specimens had lower initial elastic moduli than the outside wall specimens. Specimens from spun-cast GCI water pipes which only sample the outside half of the wall exclude the material containing the largest graphite flakes or, in other words, these specimens excluded the largest internal defects. The specimens tested for this work sampled the inside half of the pipe wall where the largest, Class 5, graphite flakes were found explaining why the behaviour of these specimens was more similar to full wall thickness specimens tested by Makar and McDonald [20], which also included the larger graphite flakes, and some pit cast pipes which can also contain Class 5 graphite flakes [8,20,28].

Given the above discussion, the tensile stress–strain behaviour of the BS 416–2 soil pipe specimens reported here appears to be representative of exhumed spun-cast GCI water pipes bearing in mind that these specimens sampled the lowest quality part of the pipe wall. An implication of this is that external corrosion may be more damaging to spun-cast GCI water pipes than internal corrosion because it removes the best quality, stronger, cast iron and exposes the poorer quality, weaker, cast iron closer to the inside wall to higher stresses.

In summary, the new BS416-2 soil pipes were found to have graphite microstructures and tensile stress–strain properties representative of exhumed spun-cast GCI water pipes making them an appropriate alternative to exhumed pipes for small-scale destructive tests. This agrees with the finding of John et al. [31] that the uniaxial fatigue properties of the new BS416-2 soil pipes are very similar to exhumed GCI pipes. The ability to use new BS416-2 soil pipes for testing is particularly beneficial where large numbers of uncorroded pipes with relatively consistent material properties are required. As a result, the following discussion of the BS416-2 soil pipe fatigue results can be considered representative of in-service spun-cast GCI water pipes.

5.2. Fatigue specimen fracture surface analysis

The good agreement between the measured fracture surface light grey region length and the predicted critical crack length shown by Fig. 12 indicates that the light grey regions correspond to the extent of stable fatigue crack growth before fast fracture occurred.

Where present, all stable crack growth regions penetrated the full way through the specimen's wall, as shown by Fig. 10, making it likely that these cracks would enable leakage before failure if they occurred in a water pipe. This is supported by the experimental observations reported by Rathnayaka *et al.* [16] of leaking cracks in pressurised water pipes prior to burst, although those cracks were generated through static rather than fatigue loading. As a result, the failure mode corresponding to the years-to-failure predictions in this study is fast fracture, or burst, preceded by a period of leakage.

Given that the maximum normal stress amplitude in the modelled years-to-failure scenario, caused by internal pressure loading, acted in the pipe's circumferential direction an axial crack orientation would be expected. As a result, fast fracture in this scenario would be expected to result in a long axial split in the pipe, rather than the circumferential splits shown by Fig. 9.

Fig. 13 shows that larger stable crack sizes prior to failure are possible at longer fatigue lives, likely due to the lower maximum stress applied to the cracks. Fig. 13 also shows that in general no stable crack growth region was discernible for fatigue lives less than about 4×10^3 cycles under R=-1 loading and 2×10^4 cycles under R=0.1 loading. The implication of this is the GCI water pipes which take more stress cycles to fail may develop larger leaking fatigue cracks prior to failure and, conversely, pipes which require fewer stress cycles to fail may not leak before failure. The variable amplitude nature of real water pipe loading is likely to complicate this picture, however.

5.3. Years-to-failure predictions

The average predicted years-to-failure for the scenario considered was 59.4 years, but this value was very sensitive to corrosion rate so must be treated with caution. Barton *et al.* [5] reported GCI pipe failures for a UK water utility in the period between 2005 and 2018. The shortest reported lifespans were between approximately 45 years and 78 years, and the highest failure rate occurred for pipes with lifespans between about 65 years and 98 years. Therefore, the average years-to-failure prediction of 59.4 years represents a realistic value.

On average, accumulated fatigue damage was predicted to exceed 0.01 after 56.0 years and a further 3.5 years were required for accumulated damage to reach unity, as shown by Fig. 17. In other words, in nearly all cases effectively no fatigue damage was predicted to have accumulated during the first 50 years. This is because for most of a pipe's life the applied stress amplitude was much too small to cause fatigue damage, so damage accumulation was only predicted to begin once wall loss due to corrosion was great enough that the stress amplitude exceeded the pipe's fatigue strength. The accumulation of fatigue damage represented a small part of the pipe's life so the predicted failure window was small relative to the pipe's life but large relative to the actual time spent accumulating fatigue damage. An implication of this short window of fatigue damage accumulation is that years-to-failure predictions can be made without knowing, or having to estimate, the loading applied early in a pipe's life.

Given the fracture surface observations discussed above, a through wall crack allowing leakage would be expected to form at some point prior to the predicted years-to-failure. It was not possible to estimate exactly when such a leaking crack would form, however, the accumulation of fatigue damage corresponds to the development of a fatigue crack. Therefore, a leaking crack would be very unlikely to form before the cumulative fatigue damage exceeded 0.01. As a result, on average, the period of leakage prior to failure in the scenario considered could be no more than 3.5 years, and would likely be much shorter.

The last GCI water pipes were laid in the UK in the 1960 s [6], so at the time of writing all remaining GCI water pipes have been in service for at least 53 years. Towards the end of a pipeline's life the variation in predicted years-to-failure caused by fatigue strength

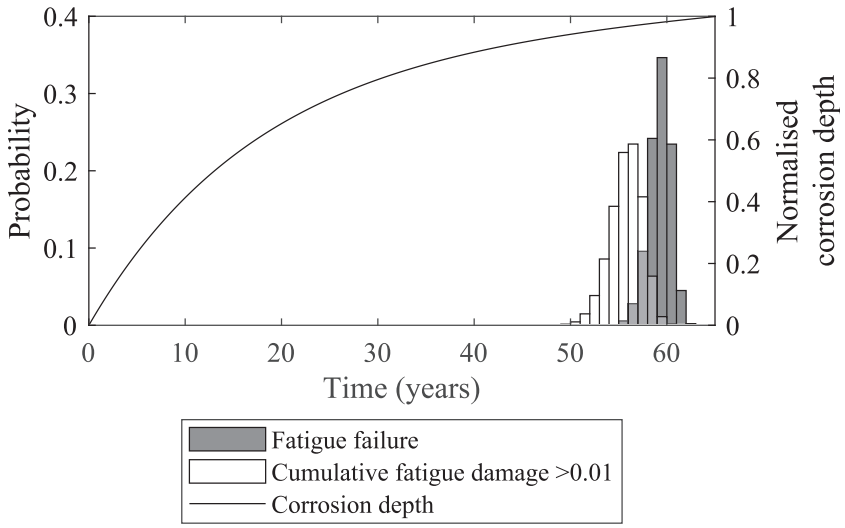

Fig. 17. Histogram showing the distributions of predicted years-to-failure and the year in which accumulated fatigue damage was predicted to exceed 0.01. The probability of occurrence for this histogram is shown by the left-hand ordinate. The predicted corrosion depth normalised by original wall thickness is also plotted with values shown by the right-hand ordinate.

variation is more significant. For the scenario modelled by this study, after an arbitrary 53 years the average predicted years-to-failure was 6.4 years, however, the distribution indicated a small chance of failure after 1 year (see Fig. 16). This difference could easily represent some pipes in a pipeline failing prior to replacement of the pipeline if the average result was used to determine the asset replacement schedule. In the UK, water utilities budget for pipe replacements in 5-year asset management plan (AMP) periods, so a 5-year variation in failure prediction could change the AMP in which pipe replacement is scheduled. While the results presented in this study represent only a single hypothetical, but realistic, scenario it seems reasonable to conclude that when using years-to-failure modelling to assess the remaining life of a GCI pipeline the variability of the pipes' fatigue strength should be considered.

The results and conclusions of this work are specific to water pipes manufactured from GCI. Although steel and Ductile Cast Iron (DCI) water pipes can fail via similar mechanisms to GCI pipes, steel and DCI pipes have different mechanical properties to GCI pipes and are also likely to have different corrosion properties [5,20]. As a result, to determine whether the findings of this paper apply to other metallic water pipes the methodology of this work should be repeated for the specific pipe material.

To account for GCI pipe fatigue strength variation in practice, a methodology similar to that presented in section 3.3 could be used by asset managers to estimate the remaining life of a pipeline. To account for the variation in fatigue strength between pipes in the pipeline, instead of using the random-draw approach, σ_A in Eq. (5) could be substituted with $\sigma_{A,P_s=90\%}$ (or σ_A for any desired probability of survival, calculated using Eq. (1) when calculating the expected years-to-failure. This would enable asset managers to schedule pipe replacement based on a specific probability of failure. This approach would ideally require fatigue test data from the pipeline of interest to determine $\sigma_{A,P_s=90\%}$. Alternatively, the fatigue strength of GCI pipes may be estimated as a proportion of their UTS [18]. Using the $\sigma_{A,P_s=90\%}$ and UTS values from the test data presented in this work, $\sigma_{A,P_s=90\%}$ for a set of similar GCI pipes is expected to be approximately 0.23 times the average UTS at 10^6 cycles to failure, although this value should be used with caution. Estimating the remaining life of a pipeline also requires good estimates of the pipes' stress histories and corrosion rate. Future work should seek to validate this type of predictive methodology using data from real water distribution networks.

6. Conclusions

This study aimed to experimentally quantify the variation of fatigue strength observed within a batch of GCI pipes and assess the impact of this variation on a years-to-failure scenario. The conclusions drawn were as follows:

- BS416-2 soil pipes can be used to represent spun-cast GCI water pipes in small-scale destructive tests. This is particularly beneficial where large numbers of un-corroded pipes with relatively consistent material properties are required.
- The loads applied to a GCI pipe early in its life have a limited impact on its remaining life because the accumulation of fatigue damage is predicted to represent a very small, terminal part of a GCI pipe's life. This means that years-to-failure predictions do not need to estimate the loads applied to pipes early in their lives.
- Through-wall cracks can exist in GCI pipes prior to fatigue failure, implying that leakage before complete pipe failure is possible. In the scenario considered this leakage period was less than 3.5 years.
- When predicting the remaining years-to-failure of a GCI pipeline that is nearing the end of its life the variation in fatigue strength between the pipes should be considered, even if the pipes are nominally identical. In the scenario considered a small chance of failure was predicted 5 years before the average predicted failure year. In the context of asset management, scheduling pipeline replacement based on the average fatigue strength is likely to give time for some pipes to fail prior to replacement.

CRediT authorship contribution statement

Edward John: Writing – original draft, Investigation, Formal analysis. **Joby Boxall:** Writing – review & editing, Methodology, Conceptualization. **Richard Collins:** Writing – review & editing, Methodology, Conceptualization. **Elisabeth Bowman:** Writing – review & editing, Methodology, Conceptualization. **Luca Susmel:** Writing – review & editing, Supervision, Project administration, Methodology, Funding acquisition, Conceptualization.

Declaration of competing interest

The authors declare that they have no known competing financial interests or personal relationships that could have appeared to influence the work reported in this paper.

Data availability

Data will be made available on request.

Acknowledgements

This work was funded by UK Water Industry Research (UKWIR) and the ESPRC through the Water Infrastructure and Resilience (WIRe) Centre for Doctoral Training (EP/S023666/1). The authors would like to thank the technicians Paul Blackbourne, Mario Dorna, Tesoro Monaghan, Chris Todd, and Richard Kay for their work which enabled the fatigue testing to take place. For the purpose of open

References

[1] J. Sanders, D. Marshallsay, G. Mountfort, G. Fox, M. Butler, A Leakage Routemap to 2050, Water UK, London, UK, 2022. https://www.water.org.uk/news-item/milestone-leakage-routemap-to-revolutionise-the-reduction-of-leakage-from-pipes/ (accessed 15th June 2022).
[2] S. Folkman, Water main break rates in the USA and Canada: A comprehensive study, Utah State University, Buried Structures Laboratory, Logan, UT, USA, 2018. https://digitalcommons.usu.edu/cgi/viewcontent.cgi?article=1173&context=mae_facpub (accessed 25th April 2024).
[3] National Infrastructure Commission, Preparing for a drier future: England's water infrastructure needs, London, UK, 2018. https://nic.org.uk/nic-preparing-for-a-drier-future-26-april-2018/ (accessed 25th April 2024).
[4] J.B. Boxall, A. O'Hagan, S. Pooladsaz, A.J. Saul, D.M. Unwin, Estimation of burst rates in water distribution mains, Proc. Inst. Civ. Eng. Water Manage. 160 (2) (2007) 73–82, https://doi.org/10.1680/wama.2007.160.2.73.
[5] N.A. Barton, T.A. Farewell, S.H. Hallett, T.F. Acland, Improving pipe failure predictions: factors effecting pipe failure in drinking water networks, Water Res. 164 (2019) 114926, https://doi.org/10.1016/j.watres.2019.114926.
[6] UK Water Industry Research, Water Industry Information & Guidance Note: Ductile Iron Pipes and Fittings, UK Water Industry Research, London, UK, 2006. https://www.water.org.uk/wp-content/uploads/2018/11/ign-4-21-01.pdf (accessed 1st March 2024).
[7] Economic Insight Ltd., Options for a sustainable approach to asset maintenance and replacement, Economic Insight Ltd., London, UK, 2022. https://www.water.org.uk/news-views-publications/publications/options-sustainable-approach-asset-maintenance-and-replacement (accessed 11th September 2023).
[8] J.M. Makar, B. Rajani, Gray cast-iron water pipe metallurgy, J. Mater. Civ. Eng. 12 (3) (2000) 245, https://doi.org/10.1061/(asce)0899-1561(2000)12:3(245).
[9] M.V. Seica, J.A. Packer, Mechanical properties and strength of aged cast iron waterpipes, J. Mater. Civ. Eng. 16 (1) (2004) 69–77, https://doi.org/10.1061/(asce)0899-1561(2004)16:1(69).
[10] R. Logan, M.J. Mulheron, D.A. Jesson, P.A. Smith, T.S. Evans, N. Clay-Michael, J.T. Whiter, Graphitic corrosion of a cast iron trunk main: Implications for asset management, WIT Trans. Built Environ. 139 (2014), https://doi.org/10.2495/UW140351.
[11] K. Atkinson, J.T. Whiter, P.A. Smith, M. Mulheron, Failure of small diameter cast iron pipes, Urban Water 4 (2002) 263–271, https://doi.org/10.1016/S1462-0758(02)00004-3.
[12] K. Yamamoto, S. Mizoguti, K. Yoshimitsu, J. Kawasaki, Relation between graphitic corrosion and strength degradation of cast iron pipe, Boshoku Gijutsu 32 (3) (1983) 157–162, https://doi.org/10.3323/jcorr1974.32.3 157.
[13] M. Ahammed, R.E. Melchers, Reliability of underground pipelines subject to corrosion, J. Transp. Eng. 120 (6) (1994) 989–1002, https://doi.org/10.1061/(ASCE)0733-947X(1994)120:6(989).
[14] B. Rajani, A. Abdel-Akher, Re-assessment of resistance of cast iron pipes subjected to vertical loads and internal pressure, Eng. Struct. 45 (2012) 192–212, https://doi.org/10.1016/j.engstruct.2012.06.019.
[15] A. Fahimi, T.S. Evans, J. Farrow, D.A. Jesson, M.J. Mulheron, P.A. Smith, On the residual strength of aging cast iron trunk mains: physically-based models for asset failure, Mater. Sci. Eng. A 663 (2016) 204–212, https://doi.org/10.1016/j.msea.2016.03.029.
[16] S. Rathnayaka, B. Shannon, D. Robert, J. Kodikara, Experimental evaluation of bursting capacity of corroded grey cast iron water pipeline, Struct. Infrastruct. Eng. 13 (12) (2017) 1553–1562, https://doi.org/10.1080/15732479.2017.1303840.
[17] W. Brevis, L. Susmel, J.B. Boxall, Investigating in-service failures of water pipes from a multiaxial notch fatigue point of view: a conceptual study, Proc. Inst. Mech. Eng. C J. Mech. Eng. Sci. 229 (7) (2015) 1240–1259, https://doi.org/10.1177/0954406214553020.
[18] R. Jiang, S. Rathnayaka, B. Shannon, X.-L. Zhao, J. Ji, J. Kodikara, Analysis of failure initiation in corroded cast iron pipes under cyclic loading due to formation of through-wall cracks, Eng. Fail. Anal. 103 (2019) 238–248, https://doi.org/10.1016/j.engfailanal.2019.04.031.
[19] J.B. Kommers, The static and fatigue properties of some cast irons, Proc. Am. Soc. Test. Mater.. 28 (2) (1928) 174–197, https://doi.org/10.1021/ie50012a019.
[20] J.M. Makar, S.E. McDonald, Mechanical behavior of spun-cast gray iron pipe, J. Mater. Civ. Eng. 19 (10) (2007) 826–833, https://doi.org/10.1061/(ASCE)0899-1561(2007)19.
[21] D.A. Jesson, H. Mohebbi, J. Farrow, M.J. Mulheron, P.A. Smith, On the condition assessment of cast iron trunk main: the effect of microstructure and in-service graphitisation on mechanical properties in flexure, Mater. Sci. Eng. A 576 (2013) 192–201, https://doi.org/10.1016/j.msea.2013.03.061.
[22] J.A. Simmons, N.A. Hoult, I.D. Moore, Behavior assessment of exhumed cast iron pipes using distributed strain sensing, J. Pipeline Syst. Eng. Pract. 15 (1) (2024) 04023051, https://doi.org/10.1061/jpsea2.pseng-1463.
[23] British Standards Institution, BS 416-2:1990 Discharge and ventilating pipes and fittings, sand-cast or spun in cast iron - part 2: Specifications for socketless systems, British Standards Publications, London, UK, 1990.
[24] M.R. Mitchell, Effects of graphite morphology, matrix hardness, and structure on the fatigue resistance of gray cast iron, SAE International (1975). Report No. 750198.
[25] British Standards Institution, BS 78:1917 Specification for cast iron pipes and special castings for water, gas and sewage, British Standards Publications, London, UK, 1917.
[26] British Standards Institution, BS 1211:1958 Centrifugally cast (spun) iron pressure pipes for water, gas & sewage, British Standards Institution, London, UK, 1958.
[27] ASTM, A247-19 Standard test method for evaluating the microstructure of graphite in iron castings, ASTM International, West Conshohocken, PA, USA, 2019. DOI: 10.1520/A0247-19.
[28] H. Mohebbi, D.A. Jesson, M.J. Mulheron, P.A. Smith, The fracture and fatigue properties of cast irons used for trunk mains in the water industry, Mater. Sci. Eng. A 527 (2010) 5915–5923, https://doi.org/10.1016/j.msea.2010.05.071.
[29] H.M. Belmonte, M. Mulheron, P.A. Smith, Weibull analysis, extrapolations and implications for condition assessment of cast iron water mains, Fatigue Fract. Eng. Mater. Struct. 30 (2007) 964–990, https://doi.org/10.1111/j.1460-2695.2007.01167.x.
[30] Hargreaves Foundry, Mech 416 Cast Iron Mechanically Jointed Soil System. https://www.hargreavesfoundry.co.uk/cast_iron_drainage/mech416/ (accessed Sep. 06, 2021).
[31] E. John, J.B. Boxall, R. Collins, E. Bowman, L. Susmel, Multiaxial fatigue of water pipe grey cast iron, Int. J. Fatigue 178 (2024) 108002, https://doi.org/10.1016/j.ijfatigue.2023.108002.
[32] MathWorks, MatLab R2021b, September 22, 2021.
[33] R.E. Little, ASTM STP 588: Manual on statistical planning and analysis for fatigue experiments, ASTM International, PA, USA, 1975. DOI: 10.1520/STP588-EB.
[34] ASTM International, ASTM E739-10: Standard Practice for Statistical Analysis of Linear or Linearized Stress-Life (S-N) and Strain-Life (ε-N) Fatigue Data, ASTM International, West Conshohocken, PA, United States, 2015. DOI: 10.1520/E0739-10R15.
[35] ASTM International, STP 91: A guide for fatigue testing and the statistical analysis of fatigue data, ASTM International, West Conshohocken, PA, United States, 1963. DOI: 10.1520/STP91A-EB.
[36] D.C. Montgomery, E.A. Peck, G.G. Vining, Introduction to linear regression analysis, fifth edn., John Wiley & Sons Inc, Hoboken, NJ, USA, 2012.
[37] S. Lampman, Fatigue and fracture properties of cast irons, ASM Handbook. 19 (1996) 665–679.
[38] D. Taylor, M. Hughes, D. Allen, Notch fatigue behaviour in cast irons explained using a fracture mechanics approach, Int. J. Fatigue 18 (7) (1996) 439–445, https://doi.org/10.1016/0142-1123(96)00018-7.
[39] W.D. Pilkey, D.F. Pilkey, Peterson's stress concentration factors, third edn., John Wiley & Sons Inc, Hoboken, NJ, USA, 2008.
[40] B. Rajani, J.M. Makar, S. McDonald, C. Zhan, S. Kuraoka, C.-K. Jen, M. Viens, Investigation of grey cast iron water mains to develop a methodology for estimating service life, American Water Works Association Research Foundation, Denver, CO, USA, 2000.

[41] H. Rezaei, B. Ryan, I. Stoianov, Pipe failure analysis and impact of dynamic hydraulic conditions in water supply networks, Procedia Eng. 119 (1) (2015) 253–262, https://doi.org/10.1016/j.proeng.2015.08.883.
[42] J. Fash, D.F. Socie, Fatigue behaviour and mean effects in grey cast iron, Int. J. Fatigue 4 (3) (1982) 137–142, https://doi.org/10.1016/0142-1123(82)90040-8.
[43] K.N. Smith, T.H. Topper, P. Watson, A stress–strain function for the fatigue of metals, J. Mater. 5 (4) (1970) 767–778.
[44] Y.-L. Lee, J. Pan, R.B. Hathaway, M.E. Barkey, Fatigue testing and analysis: theory and practice, first edn., Elsevier Butterworth-Heinemann, Burlington, MA, USA, 2005.
[45] C.M. Sonsino, Course of SN-curves especially in the high-cycle fatigue regime with regard to component design and safety, Int. J. Fatigue. 29 (12) (2007) 2246–2258, https://doi.org/10.1016/j.ijfatigue.2006.11.015.
[46] M. Janssen, J. Zuidema, R.J.H. Wanhill, Fracture mechanics, second ed., Spon Press, London, UK, New York, 2004.